ELSEVIER

Biophysical Chemistry 127 (2007) 9–18

Biophysical Chemistry

http://www.elsevier.com/locate/biophyschem

The study of amorphous aggregation of tobacco mosaic virus coat protein by dynamic light scattering

Yuliy Panyukov [a,b], Igor Yudin [c], Vladimir Drachev [a], Evgeny Dobrov [a,*], Boris Kurganov [d]

[a] *A.N. Belozersky Institute of Physico-Chemical Biology, Moscow State University, Moscow 119992, Russia*
[b] *Faculty of Bioengineering and Bioinformatics, Moscow State University, Moscow 119992, Russia*
[c] *Oil and Gas Research Institute, Russian Academy of Sciences, Gubkina St., 3, Moscow 117971, Russia*
[d] *A.N. Bach Institute of Biochemistry, Russian Academy of Sciences, Leninsky pr. 33, Moscow 119071, Russia*

Received 12 July 2006; received in revised form 23 November 2006; accepted 27 November 2006
Available online 1 December 2006

Abstract

The kinetics of heat-induced and cetyltrimethylammonium bromide induced amorphous aggregation of tobacco mosaic virus coat protein in Na^+/Na^+ phosphate buffer, pH 8.0, have been studied using dynamic light scattering. In the case of thermal aggregation (52 °C) the character of the dependence of the hydrodynamic radius (R_h) on time indicates that at certain instant the population of aggregates is split into two components. The size of the aggregates of one kind remains practically constant in time, whereas the size of aggregates of other kind increases monotonously in time reaching the values characteristic of aggregates prone to precipitation (R_h=900–1500 nm). The construction of the light scattering intensity *versus* R_h plots shows that the large aggregates (the start aggregates) exist in the system at the instant the initial increase in the light scattering intensity is observed. For thermal aggregation the R_h value for the start aggregates is independent of the protein concentration and equal to 21.6 nm. In the case of the surfactant-induced aggregation (at 25 °C) no splitting of the aggregates into two components is observed and the size of the start aggregates turns out to be much larger (107 nm) than on the thermal aggregation. The dependence of R_h on time for both heat-induced aggregation and surfactant-induced aggregation after a lapse of time follows the power law indicating that the aggregation process proceeds in the kinetic regime of diffusion-limited cluster–cluster aggregation. Fractal dimension is close to 1.8. The molecular chaperone α-crystallin does not affect the kinetics of tobacco mosaic virus coat protein thermal aggregation.

Keywords: Tobacco mosaic virus coat protein; Amorphous aggregation; Cetyltrimethylammonium bromide; Dynamic light scattering

1. Introduction

Amorphous (unordered) aggregates of different proteins have been recently implicated in pathogenesis of many important human diseases [1–5]. However, structural studies of such aggregates are greatly hampered by their large size, transient character, and heterogeneity. Probably, because of this, up to now, as far as we know, only one detailed model of mechanism of amorphous protein aggregation has been proposed. This is the Goldberg–Wetzel model [6,7] according to which unordered aggregates are formed by intermolecular interactions of those domains of partly disordered protein molecules, which in the native state were involved in intramolecular interactions between the same domains.

Tobacco mosaic virus (TMV) coat protein (CP) is well known for its ability to produce ordered assemblies [8]. It is well known that at room temperature, pH values in the range from 7.5 to 9.0, and ionic strength in the range from 10 to 100 mM, the TMV CP exists in the form of so called 4S-protein (a dynamic mixture of pentamers and trimers, with a minor amount of monomers). At pH of about 7.0 and ionic strength of about 100 mM TMV CP with high efficiency specifically assembles *in vitro* with TMV RNA with formation of completely native virions. At pH ≤ 6.0 in the absence of RNA, the protein produces long virus-like helical aggregates called repolymerized protein [8].

However, TMV CP also turned out to be a good model for studies of thermal amorphous aggregation. In contrast to most

* Corresponding author. Tel.: +7 495 9395008; fax: +7 495 9393181.
E-mail address: dobrov@belozersky.msu.ru (E. Dobrov).

0301-4622/$ - see front matter © 2006 Elsevier B.V. All rights reserved.
doi:10.1016/j.bpc.2006.11.006

of other unspecific protein aggregation system [7,9], the process of amorphous TMV CP aggregation is highly reproducible and its rate can be easily manipulated by changing solution ionic strength, protein concentration, and temperature [10–13]. Recently we have observed that the TMV CP amorphous aggregation can be also induced in neutral phosphate buffer (PB) at room temperature (25 °C) by low micromolar concentrations of cationic surfactant cetyltrimethylammonium bromide (CTAB) [14].

And finally, possible existence of amyloidogenic potential in TMV CP have been suggested by R. Diaz-Avalos and D. Caspar from the results of their studies of the TMV CP "off-pathway" aggregate (stacked disks) structure [15].

Dynamic light scattering (DLS) gives valuable information on the size of protein aggregates and is widely used for the study of the kinetics of protein aggregation. DLS, as applied to analysis of protein aggregates, has some evident merits. Modern variants of DLS technique allow registering the initial stages of protein aggregation, where the fraction of the aggregated protein constitutes some tenth of a percent of the total amount of the protein in the system. Besides, this method allows quantitative determination of the individual components in heterogeneous populations of aggregates [16–26].

Recently we have studied with the help of DLS the process of aggregation of β_L-crystallin in the presence of α-crystallin. We have found that three different types of amorphous aggregates (named "start aggregates", "basic aggregates" and "superaggregates") are formed [27]. The construction of the light scattering intensity *versus* hydrodynamic radius plot allows estimating the size of the start aggregates [27]. The formation of the start aggregates (the primary clusters) has been also observed on thermal aggregation of several other proteins [27–29].

The goal of the present work was to carry out the comparative study of the kinetics of irreversible heat-induced and reversible CTAB-induced amorphous aggregation of the TMV CP by DLS. It has been shown that in both cases aggregation proceeds by way of the formation of the start aggregates.

2. Experimental

2.1. TMV purification and proteins preparation

Wild-type (strain U1) TMV was obtained as described elsewhere [30] and its coat protein was isolated by the acetic acid method [31]. The CP preparations were stored at concentrations of 4.5 to 6 mg/ml (259–345 μM) in 5 mM Na^+/Na^+ PB, pH 8.0, at +4 or −20 °C. The TMV CP concentrations were measured by UV spectroscopy using the extinction coefficient $A_{280}^{0.1\%}$ of 1.30 [32].

α-Crystallin from bovine eye lenses was purchased from Sigma (USA).

2.2. DLS measurements

DLS is widely used in biochemistry to measure the size of particles suspended in liquids [16–29,33]. Measured value of the decay rate τ_c of the light scattering intensity fluctuations allows finding the diffusion coefficient D of the particles using expression [34]:

$$D = \frac{1}{2\tau_c k^2}, \quad (1)$$

where k is the wave number of the scattered light, $k = \frac{2\pi n}{\lambda}\sin\frac{\theta}{2}$, n is the refractive index of the solvent, λ is the wavelength of the incident light in vacuum, and θ is the scattering angle. The mean hydrodynamic radius of the particles, R_h, can then be calculated according to the Stokes–Einstein equation:

$$D = \frac{k_B T}{6\pi\eta R_h}, \quad (2)$$

where k_B is Boltzmann's constant, T is the temperature, and η is the shear viscosity of the solvent.

The commercial DLS setup Photocor Complex (Photocor Instruments Inc., USA; www.photocor.com) was used throughout this work. A He–Ne laser (Coherent, USA, Model 31–2082, 632.8 nm, 10 mW) is used as a light source. The temperature of sample cell was controlled by the temperature controller to within ±0.1 °C. To improve accuracy of measurements of small particles (~ 1 nm), a quasi-cross correlation photon counting system with two photomultipliers with high quantum efficiency (12% at 633 nm) was used (Hamamatsu Photonics, Japan, model R6358P). The correlation function of light scattering fluctuations was analyzed by a universal correlator Photocor-FC, which has both multiple-tau and linear time-scale mode. Operation of the correlator in multiple-tau mode needs no tuning of time-scale and is suitable for measurements of multi-peak particle distributions as well for the sizing of growing particles in the course of aggregation. A number of preliminary experiments have been done to find optimal accumulation times. Depending on the observed aggregation kinetics, the typical accumulation times were chosen to be 1–2 min. Taking into account relatively small particle sizes and low scattering intensities corresponding to such short times we obtained only mean sizes of particles with unimodal or bimodal distribution. Polydispersity analysis was performed using DynaLS software (Alango, Israel). DynaLS program uses original algorithms based on the well-known regularization approach.

All DLS equipment and data processing were the same as the ones used in our previous work [27].

2.3. The kinetics of thermal amorphous aggregation of TMV CP

50 mM PB was placed in a cylindrical cell with the diameter of 14.5 mm and preincubated for 10 min at 52 °C. The aggregation process was started by the addition of a small aliquot of preheated at 35 °C TMV CP to the final volume of 1 ml. When testing the effect of α-crystallin on the thermal aggregation of TMV CP, 10 min preincubation of the 50 mM PB was carried on in the presence of α-crystallin (final concentration 1 mg/ml).

2.4. The kinetics of CTAB-induced amorphous aggregation of TMV CP

Aliquots of TMV CP in 10 mM PB were placed in a cylindrical cell and preincubated at 25 °C. The aggregation process was started by the addition of small aliquots of 2 mM CTAB to the final volume of 1 ml.

2.5. The dependence of initial rates of turbidity increase (v_{in}) on the solution ionic strength

The turbidity changes in the case of CTAB-induced TMV CP amorphous aggregation were monitored at 320 nm (A_{320}) in 1 cm cell using UV–Vis spectrophotometer SLM Aminco DW-2000 (SLM Instruments Inc., USA). Aliquots of TMV CP in PB of various molarities were placed in cell and preincubated at 25 °C. The aggregation process was started by the addition of small aliquots of 2 mM CTAB to the final volume of 2 ml. The initial rates of the A_{320} increase (v_{in}) were calculated in absorbance units per minute from the linear portion of the kinetic curves.

The dependence of v_{in} on the solution ionic strength for the heat-induced TMV CP aggregation is taken from our previous paper [10].

3. Results

3.1. The kinetics of thermal aggregation of TMV CP

Dynamic light scattering allows the changes in the size of aggregates in the course of protein aggregation to be registered. Fig. 1 shows the typical autocorrelation functions measured at various times of incubation of 5.75 μM (0.1 mg/ml) TMV CP in 50 mM PB at 52 °C. Using the DynaLS software we calculated the size distribution of particles formed in the course of aggregation. At sufficiently short times of incubation the distribution function was unimodal (Fig. 2A, B). The mean value of the hydrodynamic radius (R_h) increased with the time of incubation. At times of incubation longer than 22 min, in addition to the main TMV CP aggregates, the aggregates of a larger size appeared and the aggregate R_h distribution became

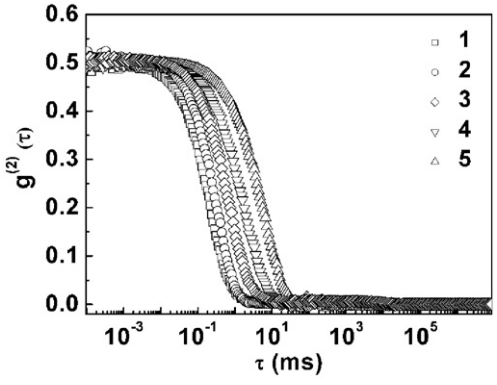

Fig. 1. Autocorrelation functions measured at various times of incubation of 5.75 μM TMV CP (50 mM PB) at 52 °C: (1) 5, (2) 10, (3) 22, (4) 45, (5) 75 min. All curves were measured at scattering angle of 90°.

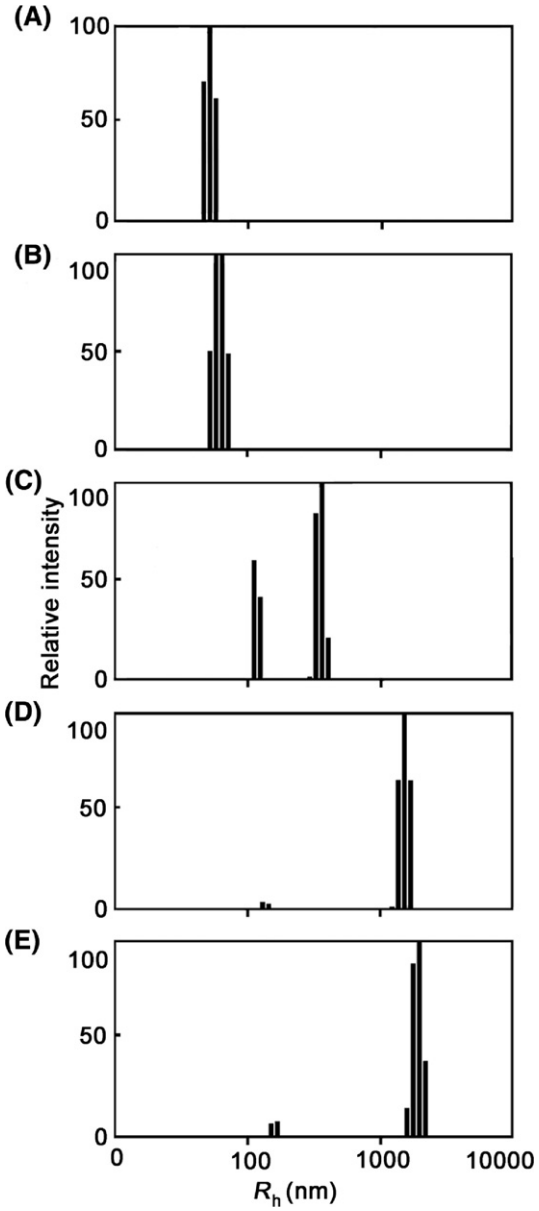

Fig. 2. Aggregation of 5.75 μM TMV CP (50 mM PB) at 52 °C. The distribution of the particles with their size registered at various times of incubation: (A) 5, (B) 10, (C) 22, (D) 45, (E) 75 min. R_h is the hydrodynamic radius.

bimodal (Fig. 2C–E). The R_h of the large-sized aggregates increased monotonously with the time of incubation, while the R_h of the main aggregates remained constant. Small variations in the peak positions for small particles are a result of some ambiguity in the polydispersity analysis.

The process of thermal amorphous aggregation of TMV CP at 52 °C is accompanied by an increase in the light scattering intensity. Fig. 3A and C show the time-course of the light scattering intensity obtained at two concentrations of TMV CP (2.88 and 5.75 μM); the kinetic curves are shown in the time intervals of 0–180 and 0–60 min, respectively. At sufficiently long incubation times the light scattering intensity approached the limiting value. In the time interval, where the increment of the light scattering intensity is observed, the distribution of the aggregates with their size remained

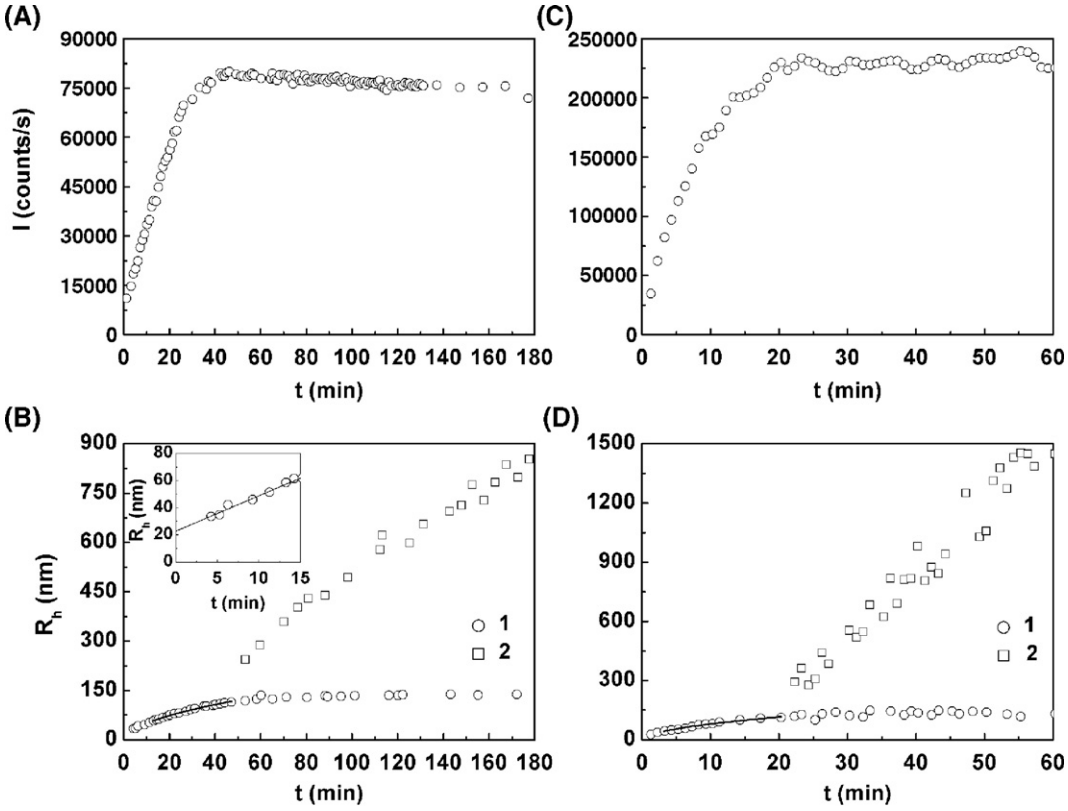

Fig. 3. The kinetics of thermal aggregation of TMV CP at 52 °C. The protein concentration: (A) and (B) 2.88 μM, (C) and (D) 5.75 μM. (A) and (C) the dependence of the intensity of light scattering on time. (B) and (D) the dependence of the hydrodynamic radius (R_h) of the basic aggregates (1) and superaggregates (2) on time. The solid curves are drawn in accordance with Eq. (4). Inset in panel (B) shows the initial part of the dependence of R_h on time.

unimodal and the R_h value increased with increasing time of incubation (Fig. 3B and D). We shall call the aggregates existing when the increment of the light scattering intensity is observed "basic aggregates". At both protein concentrations the splitting of the aggregate population into two components occurred at the time points (~ 50 and ~ 20 min, respectively), where the light scattering intensity stopped to increase. The size of the aggregates of one kind (basic aggregates) remained constant in time (R_h = 135 nm). The size of the aggregates of other kind ("superaggregates") increased monotonously till the values (R_h = 900–1500 nm) characteristic of the large-sized aggregates prone to precipitation.

The appearance of high R_h superaggregates of course results in increase in the light scattering intensity. However, although the size of superaggregates increases, their number (concentration) decreases due to sticking, and the total scattering intensity should be saturated for particles with the size of 900 to 1500 nm. Also, in aggregation phenomena one more effect may appear. Particles with R_h > 1000 nm may sediment in the course of experiment and the real particle size distribution in scattering volume may change. Concentration of smaller particles increases compared with concentration of larger particles. This effect too can cause saturation of the light scattering intensity dependence.

The simultaneous measurement of the light scattering intensity (I) and hydrodynamic radius (R_h) in the course of aggregation of TMV CP allows constructing the I *versus* R_h plots. Fig. 4 shows the light scattering intensity *versus* hydrodynamic radius plots obtained at various concentrations of TMV CP in the range from 1.44 to 8.63 μM (52 °C). All these dependence are linear. As can be seen from Fig. 4, the sufficiently large, so called, start aggregates already exist in this system at the moment when the initial increase in the light scattering intensity is observed. The hydrodynamic radius of the start aggregates ($R_{h,0}$) can be estimated as a length cut off on the abscissa axis by the linear dependence of the light scattering intensity on R_h. The $R_{h,0}$ values for the TMV CP thermal aggregation determined in this way turned out to be independent

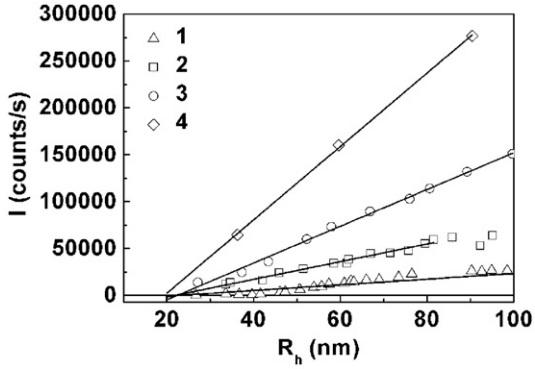

Fig. 4. The dependence of the light scattering intensity on the hydrodynamic radius (R_h) obtained at various concentrations of TMV CP: (1) 1.44, (2) 2.88, (3) 5.75, (4) 8.63 μM (50 mM PB, 52 °C).

Table 1
The parameters of the heat-induced TMV CP amorphous aggregation

Concentration of TMV CP (μM)	$R_{h,0}$ [a] (nm)	$R_{h,0}$ [b] (nm)	t_{2R} (min)	t^* (min)	R_h^* (nm)	K_1 (min^{-1})	d_f
1.44	22.6±1.0	23.5±0.5	0.41±0.02	10.1	41.9	0.039±0.004	1.80±0.06
2.88	21.9±0.6	22.8±1.1	0.38±0.01	12.8	58.5	0.072±0.014	1.79±0.08
5.75	22.4±0.5	20.6±1.2	0.156±0.002	3.3	42.5	0.33±0.07	1.80±0.07
8.63	19.4±0.3	–	–	–	–	1.6±0.6	1.80±0.3
Mean values	21.6±1.1	21.6±1.1	–	–	–	–	1.80±0.078

[a] $R_{h,0}$ values determined by extrapolation of the *I versus* R_h plots.
[b] $R_{h,0}$ values calculated by extrapolation of the dependence of R_h on time using Eq. (3).

of the protein concentration and the mean value of $R_{h,0}$ was 21.6±1.1 nm (Table 1).

Analysis of the dependence of R_h on time shows that this dependence consists of two parts. The initial part is described by the linear function:

$$R_h = R_{h,0}\left(1 + \frac{1}{t_{2R}}t\right), \quad (3)$$

where $R_{h,0}$ corresponds to the size of the start aggregates and t_{2R} is the time the hydrodynamic radius taken to reach the value of $2R_{h,0}$. Parameter t_{2R} characterizes the rate of aggregation. The lower the value of t_{2R}, the higher the rate of aggregation. Inset in Fig. 3B demonstrates the applicability of this linear function for description of the initial part of the dependence of R_h on time (2.88 μM TMV CP). The values of $R_{h,0}$ determined by the extrapolation of the dependence of R_h on time to $t=0$ coincide with the corresponding values estimated from the light scattering intensity *versus* R_h plots (Table 1). The increase in the concentration of TMV CP in the interval from 1.44 to 5.75 μM is accompanied by the 2.6-fold decrease in the t_{2R} value.

At longer times ($t>t^*$) the dependence of R_h on time changes to the power law:

$$R_h = R_h^*[1 + K_1(t-t^*)]^{1/d_f}, \quad (4)$$

where R_h^* is the value of R_h at $t=t^*$, K_1 is a constant, d_f is the fractal dimension. Going from the linear dependence of R_h on time to the power law is typical of the regime of diffusion-limited cluster–cluster aggregation (the regime wherein the rate of aggregation is limited by diffusion of the colliding particles) [35–38]. For this regime of aggregation at rather high values of time the dependence of R_h on time follows the following law:

$$R_h = R_{h,0}(1 + K_1 t)^{1/d_f}, \quad (5)$$

where $R_{h,0}$ is the hydrodynamic radius of a seed particle. The fractal dimension is a structural characteristic of aggregates.

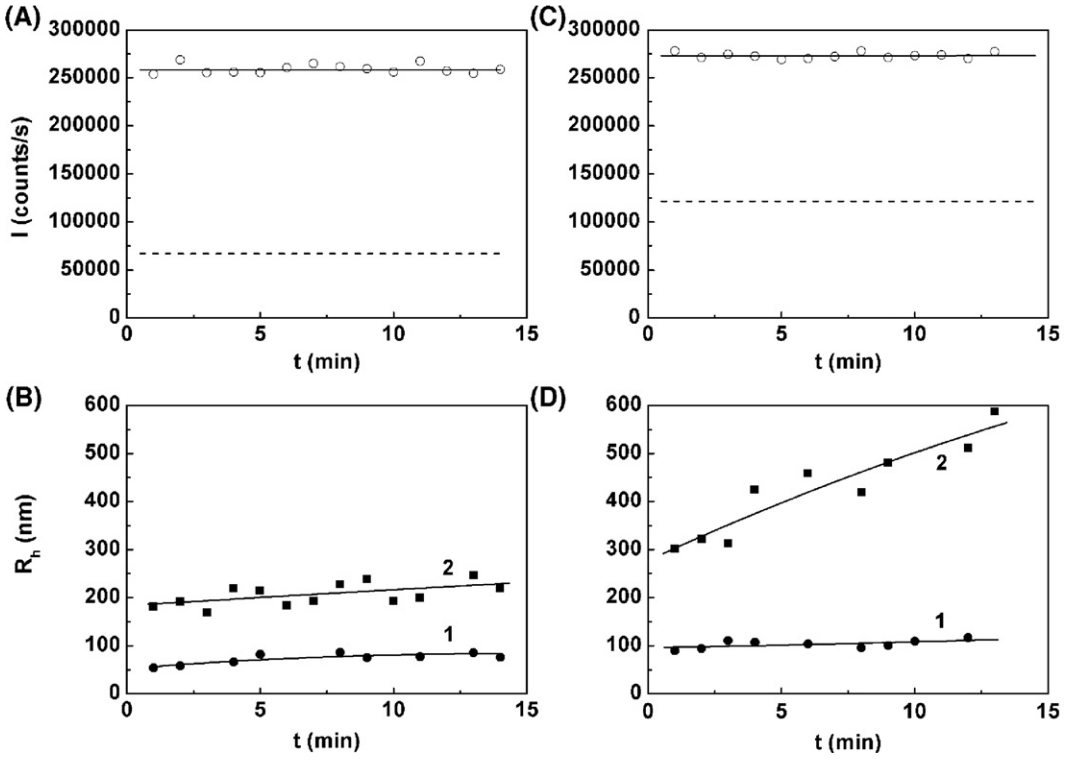

Fig. 5. The stability of the TMV CP basic aggregates at 25 °C. TMV CP (5.75 μM) was incubated for 2.5 min (A and B) and 6 min (C and D) at 52 °C in 50 mM PB and then quickly cooled to 25 °C. The time dependence of the light scattering intensity (A and C) and the hydrodynamic radius (B and D) for the cooled samples were measured at 25 °C. The dotted lines in (A) and (C) correspond to the initial values of the light scattering intensity of the protein samples after 2.5 and 6 min incubation at 52 °C. Curves (1) and (2) in (B) and (D) correspond to the basic aggregates and superaggregates, respectively.

The mass of an aggregate (M) formed as a result of unordered interactions (random aggregation) is connected with its effective radius (R) by the following relationship: $M \sim R^{d_f}$. For aggregation proceeding in the regime of diffusion-limited cluster–cluster aggregation a universal fractal dimension of 1.8 is observed [35–38].

R_h^* and t^* are the coordinates of the points where the linear parts of the curves end. The systems which we have studied (protein aggregation) differ rather strongly from the systems for which diffusion-limited cluster–cluster aggregation regime ($d_f = 1.8$) were initially developed. In those systems aggregation-prone particles exist from the start of the process ($t = 0$). However, in our case, protein molecules first are denatured, then they form start aggregates and only then the start aggregates begin to stick together with the increase in scattering intensity. Thus, the period of start aggregate formation should exist and only at times longer than t^* the intensity increase should obey diffusion-limited cluster–cluster aggregation model ($d_f = 1.8$).

The experimental dependence of R_h on time obtained at various concentrations of TMV CP (Fig. 3) were analyzed using Eq. (4) for time interval $t > t^*$. Parameters obtained (K_1 and d_f) are given in Table 1. The values of d_f are close to the universal value of fractal dimension ($d_f \approx 1.8$) typical of diffusion-limited cluster–cluster aggregation. In the interval of TMV CP concentrations from 1.44 to 8.63 μM 40-fold increase in K_1 value is observed (Table 1).

3.2. The stability of the TMV CP basic aggregates

To check the stability of the basic aggregates of TMV CP the following experiments were carried out. The incubation times were chosen so, as to be in the interval where only the basic aggregates are formed, namely, 2.5 min (Fig. 5A, B) and 6 min (Fig. 5C, D). After heating of 5.75 μM TMV CP (50 mM PB) at 52 °C for these periods of time the protein samples were quickly cooled to 25 °C and the DLS measurements were performed for 15 min at 25 °C. Cooling the protein samples from 52 to 25 °C resulted in the marked increase in the intensity of light scattering (Fig. 5A and C). As can be seen in Fig. 5B and D, this increase in the light scattering intensity is due to the formation of the large-sized aggregates. (The aggregates of a lesser size in Fig. 5B and D (curves 1) are the basic aggregates.) The R_h value for the basic aggregates increased only slightly with time during incubation at 25 °C, while the size of the superaggregates rose rather strongly (curve 2 in Fig. 5D). It is reasonable to assume that the large-sized aggregates are formed by sticking together of the basic aggregates. As can be seen from Fig. 5B and D, smaller basic aggregates formed on 2.5 min-heating at 52 °C ($R_h = 55$ nm) displayed a lower tendency for superaggregation than the larger aggregates formed on 6.5 min-heating at 52 °C ($R_h = 90$ nm). In DLS experiments we never observed breakdown of the basic TMV CP aggregates on cooling from 52 to 25 °C. We did not find any further changes in R_h after longer times of incubation. These findings are indicative of the irreversible character of amorphous aggregation of TMV CP and agree with data obtained previously [10].

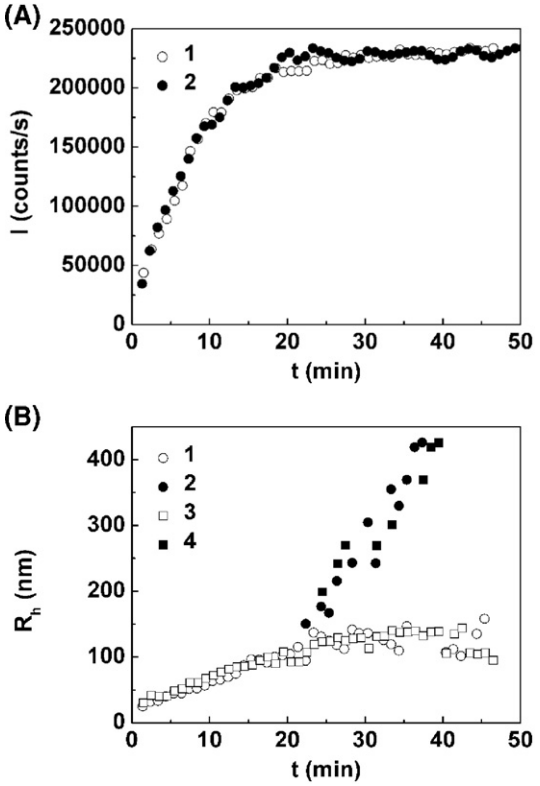

Fig. 6. Effect of α-crystallin on the kinetics of thermal aggregation of 5.75 μM (0.1 mg/ml) TMV CP (50 mM PB) at 52 °C. (A) The dependence of the intensity of light scattering on time in the absence of α-crystallin (1) and in the presence of 1 mg/ml α-crystallin (2). (B) The dependence of the hydrodynamic radius (R_h) of the basic aggregates (1 and 3) and superaggregates (2 and 4) on time. The concentration of α-crystallin: (1) and (2) 0 mg/ml and (3) and (4) 1 mg/ml.

3.3. Thermal aggregation of TMV CP in the presence of α-crystallin

α-Crystallin, the major protein of the mammalian lens, exhibits the chaperone-like properties, suppressing aggregation of denatured proteins [39]. This function is important for the maintenance of lens transparency and prevention of cataract [40–42]. We decided to test the effect of α-crystallin on TMV CP thermal amorphous aggregation. The kinetics of aggregation of 5.75 μM (0.1 mg/ml) TMV CP at 52 °C (50 mM PB) in the absence and in the presence of α-crystallin (1 mg/ml) are shown in Fig. 6. As can be seen from the figure, the time-courses of the light scattering intensity and hydrodynamic radii do not change in the presence of α-crystallin. Thus, in these conditions α-crystallin does not affect the thermal amorphous aggregation of TMV CP.

3.4. DLS study of kinetics of CTAB-induced TMV CP amorphous aggregation

Recently we have found that low concentrations of cationic surfactant cetyltrimethylammonium bromide induce amorphous aggregation of TMV CP at room temperature (25 °C) in 10 mM PB, pH 8.0. In contrast to the thermal TMV CP aggregation, the CTAB-induced aggregation occurred without

any visible changes in the protein structure [14]. Therefore, we decided to study CTAB-induced amorphous aggregation of TMV CP using DLS.

We measured the light scattering intensity and hydrodynamic radius of aggregates in the course of incubation of 11.5 μM (0.2 mg/ml) CP with various CTAB concentrations ([CTAB]:[CP] ratios from 3:1 to 5:1) at 25 °C in 10 mM PB, pH 8.0 (Fig. 7A). It was observed that the rate of the light scattering intensity increase in the course of CTAB-induced amorphous aggregation rises with the increase in the [CTAB]:[CP] ratio (Fig. 7A) and closely follows the turbidity (A_{320}) changes [14]. At the same time the kinetics of the R_h change (Fig. 7B) turned out to be the same for different [CTAB]:[CP] molar ratios. The rate of the R_h increase was independent of [CTAB]:[CP] molar ratio, R_h rose monotonously with the time, and the aggregate precipitation occurred at the final stages of the process. The divergence of *I versus t* curves for different CTAB concentrations in Fig. 7 may be explained by differences in the aggregate concentrations. This concentration rises with the increase in CTAB concentration. No splitting of the aggregate population into two components, like in the case of the TMV CP thermal aggregation (Fig. 3), was observed.

Analysis of the dependence of R_h on time shows that, as in the case of thermal aggregation of TMV CP, in the absence of surfactant, this dependence consists of linear part described by Eq. (3) and the part described by power law Eq. (4). From the common straight line combining three concentrations of CTAB

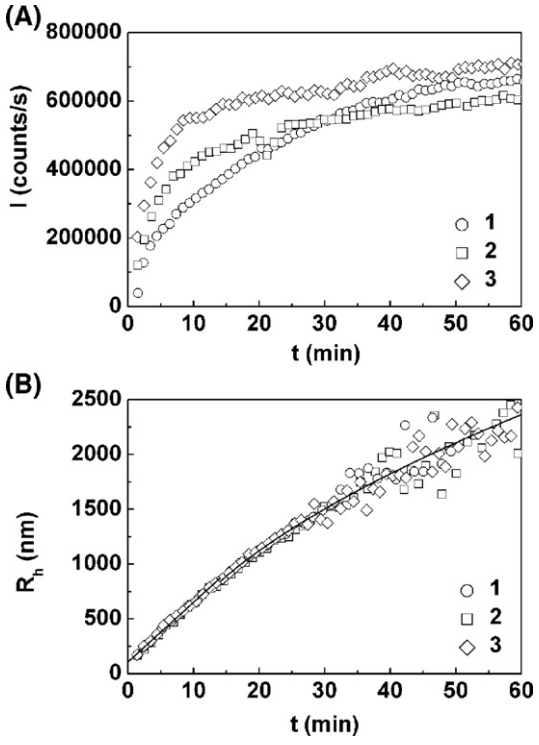

Fig. 7. The kinetics of CTAB-induced aggregation of TMV CP at various CTAB concentrations. The protein concentration is 11.5 μM. The dependence of the light scattering intensity (A) and hydrodynamic radius (R_h) (B) on time obtained at concentrations of CTAB: (1) 34.3, (2) 46, (3) 57.5 μM (10 mM PB, 25 °C). The solid curve is drawn in accordance with Eq. (3) for the interval 0–13 min and with Eq. (4) at $t>13$ min.

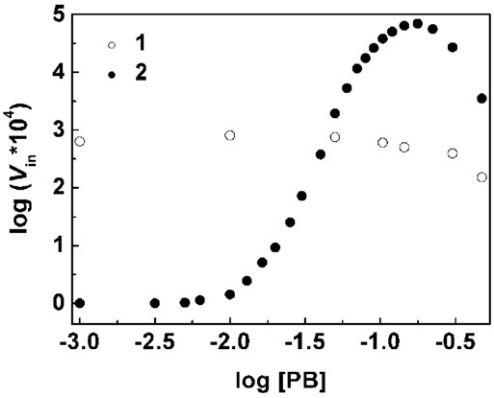

Fig. 8. The dependence of the initial rates of the A_{320} increase (v_{in}) on the solution ionic strength in the logarithmic coordinates for (1) TMV CP amorphous aggregation induced by 34.3 μM CTAB at 25 °C and (2) heat-induced TMV CP amorphous aggregation (52 °C). The protein concentration was 11.5 μM.

the following values of parameters of Eq. (3) were obtained: $R_{h,0}=107\pm3$ nm and $t_{2R}=1.96\pm0.07$ min.

At $t\geq13$ min Eq. (4) is fulfilled. The following values of parameters were obtained for the common curve: $K_1=0.123\pm0.002$ min^{-1} and $d_f=1.74\pm0.13$ ($R_h^*=785$ nm).

As mentioned above, the time dependence of increase in turbidity (A_{320}) and DLS intensity for TMV CP amorphous aggregation are similar [10,14]. Here in Fig. 8 we show the dependence of initial rates of the A_{320} increase (v_{in}) on the solution ionic strength (determined by PB molarity) in the logarithmic coordinates for heat-induced (52 °C) and CTAB-induced (25 °C) TMV CP aggregation. Previously we have reported [10] that the heat-induced aggregation is characterized by highly unusual ionic strength dependence. As can be seen from Fig. 8, v_{in} increases 1300 times in the range from 20 to 150 mM PB. We have ascribed this effect to the existence of a delicate balance between repulsive electrostatic interactions and attractive hydrophobic interactions on the surface of TMV CP molecules [10,12].

Nothing of the kind was observed in the case of CTAB-induced TMV CP aggregation (Fig. 8). In this system the initial rates of aggregation changed only slightly on four orders of magnitude increase in ionic strength, testifying to significant differences in mechanisms of the heat-induced and the CTAB-induced TMV CP aggregation.

4. Discussion

With the help of DLS it was found that two types of aggregates (basic aggregates and superaggregates) are formed in the course of the TMV CP thermal aggregation (Figs. 2 and 3). The splitting of aggregate population into two components is not a general phenomenon, but it was registered by DLS for thermal aggregation of bovine serum albumin at 58 °C [26], aggregation of dithiothreitol-denatured α-lactalbumin [43], and thermal aggregation of β_L-crystallin in the presence of α-crystallin [27]. The results of experiments on the determination of the size of the TMV CP aggregates formed by short-term heating at 52 °C,

followed by cooling to 25 °C, directly demonstrate that the large-sized superaggregates are produced by sticking together of the basic aggregates.

The DLS experiments on the kinetics of TMV CP thermal amorphous aggregation also allowed us to conclude that rather large aggregates (the start aggregates) are present even at shortest times of incubation. The size of the start aggregates was estimated from the light scattering intensity *versus* the hydrodynamic radius plots (Fig. 4; Table 1) and from Eq. (3) (Fig. 3; Table 1) [27]. The linear character of the dependence of the light scattering intensity on the hydrodynamic radius may be considered as an empiric law. We observed such a regularity for the thermal aggregation of a number of proteins [27–29]. Highly complex character of light scattering intensity dependence on particle number and structure in the course of protein aggregation makes its theoretical description especially difficult. Possible reasons of unexpected linear dependence of the light scattering intensity on the hydrodynamic radius will be a subject of further studies.

Recently we have reported that large-scale amorphous aggregation of TMV CP can be induced in usual PB at room temperature by low micromolar concentrations of cationic surfactant cetyltrimethylammonium bromide [14]. The CTAB-induced aggregation could be easily reversed by addition of anionic surfactant sodium dodecyl sulfate (SDS) due to transfer of CTAB molecules from the protein subunits to the protein free CTAB-SDS mixed micelles. This fact and the results of circular dichroism and fluorescence studies [14] suggest that completely (or almost completely) native TMV CP subunits participate in the aggregate formation. In contrast to this, the thermal TMV CP aggregation involves partially denatured protein molecules and occurs through aberrant intersubunit interactions between so called hydrophobic girdles [12]. It also should be kept in mind that the thermal TMV CP aggregation occurs in a single-component system, while the CTAB-induced aggregation in a two-component one. Besides, the first process occurs at 52 °C and the second at room temperature.

Thus, it is not surprising that DLS study also reveals important differences between the two processes. The size of the start aggregates equals 21.6 nm for the heat-induced aggregation and 107 nm for the CTAB-induced one. In the case of thermal aggregation splitting of the aggregate population into two components occurs when the basic aggregate size (R_h) reaches ~ 130 nm, and no such splitting is observed for the surfactant-induced aggregation. For the CTAB-induced aggregation the rates of R_h growth (Fig. 7B) do not correlate with the rates of light scattering intensity (I) increase (Fig. 7A). On rise in the CTAB concentration from 34.5 to 57.5 μM the initial rate of I increase rises rather strongly, while the rate of R_h increase remains the same.

The comparison of ionic strength effects on the rates of the heat-induced (52 °C) and the CTAB-induced TMV CP amorphous aggregation (Fig. 8) throws some light on possible origin of these differences. Binding of positively charged CTAB molecules neutralizes the TMV CP subunit negative charge and results in loss of the subunit electrostatic repulsion and increase in the protein molecule hydrophobicity [14]. The pure hydrophobicity driven nature of the CTAB-induced TMV CP aggregation makes its dependence on the solution ionic strength much less drastic. It should be also remembered that completely (or almost completely) native TMV CP molecules are incorporated into the CTAB-induced aggregates [14].

In our opinion, it is these differences in mechanisms of aggregation, which determine the increase in the start aggregate size and the *absence* of aggregate population splitting into two components in the case of the CTAB-induced aggregation (Fig. 7). The decrease in the start aggregate diffusion rate may also contribute to these effects. The different rates of the DLS intensity increase at different CTAB concentrations may be explained by the fact that the aggregate number rises with the increase in the surfactant concentration, while the aggregate size dynamics remains the same.

At the same time the thermal aggregation and CTAB-induced TMV CP aggregation have some common features. They include the absence of a lag period in the aggregation kinetic curves, the presence of the 13–15 min linear portion in the R_h *versus* t plots, and similar values of d_f (1.80 and 1.74 for the heat-induced and CTAB-induced aggregation, respectively; Figs. 3 and 7). Both these values are close to the value (d_f=1.75–1.80), which is typical of the protein aggregation processes proceeding in the diffusion-limited regime [35–38]. In this regime interaction of the start aggregates occurs in such a way that every collision of the particles results in their sticking.

The ability of α-crystallin to suppress protein aggregation is supposed to occur through its interaction with "non-native" hydrophobic patches exposed to the solvent upon protein unfolding. The fact that α-crystallin does not affect the kinetics of thermal amorphous aggregation of TMV CP may be indicative of the important role of specific interactions in the formation of the TMV CP aggregates. These data support our suggestion [10,12] that the TMV CP thermal amorphous aggregation is driven by distorted intersubunit interactions of those regions of the molecules, which in the native state participate in very strong intersubunit interactions leading to the formation of the ordered aggregates (helical "polymers" and virions).

Thus, it seems that mechanisms of both the heat-induced and the CTAB-induced TMV CP aggregation agree not too well with the predictions of the Goldberg–Wetzel model [6,7], that protein amorphous aggregates are formed due to specific intermolecular interactions of surfaces of the protein molecule subdomains, which are normally involved in tertiary intramolecular interactions between the same surfaces within one molecule. However, the capacity to produce highly stable ordered aggregates is the most prominent feature of the TMV CP, and the Goldberg–Wetzel model still can be true for a majority of proteins, which in their native state do not display such strong propensity for intermolecular interactions. At the same time it now gets clear that many proteins, which we had thought to work as monomolecular entities, in fact, perform their functions in the form of highly complex homo- or heteropolymeric structures.

5. Conclusions

The results of the present and previous [27–29] studies testify that in many cases amorphous protein aggregation begins with

the formation of rather large start aggregates (with the R_h value from 20 to 100 nm) and further occurs according to the diffusion-limited cluster–cluster aggregation mechanism [35–38]. Nevertheless, important differences in the process of aggregation are observed for individual systems. In the course of thermal aggregation of mixtures of β_L- and α-crystallins and of TMV CP the splitting of the aggregate populations into two components takes place, while no such splitting is registered on thermal aggregation of pure β_L-crystallin and rabbit muscle glyceraldehyde-3-phosphate dehydrogenase and on the CTAB-induced TMV CP aggregation. These systems are also characterized by different character of *I versus* R_h dependence. All these differences may be determined (among other things) by different mechanisms of aggregation (intrasubunit against intersubunit interactions) and/or by different contribution of electrostatic and hydrophobic components. Of course, theoretical description of these systems would be of a great help, but such description should be strongly aided by increasing the number of experimental systems tested out for their aggregation behavior.

Acknowledgements

This work was supported by the Russian Foundation for Basic Research (grants 05-04-49503 and 05-04-48691), the Program for Fundamental Research "Molecular and Cell Biology" of the Presidium of Russian Academy of Sciences, and INTAS (grant 03-51-4813).

References

[1] M. Bucciantini, E. Giannoni, F. Chiti, F. Baroni, L. Formigli, J. Zurdo, N. Taddei, G. Ramponi, C. Dobson, M. Stefani, Inherent toxicity of aggregates implies a common mechanism for protein misfolding diseases, Nature 416 (2002) 507–511.

[2] M. Hoshi, M. Sato, S. Matsumoto, A. Noguchi, K. Yasutake, N. Yoshida, K. Sato, Spherical aggregates of beta-amyloid (amylospheroid) show high neurotoxicity and activate tau protein kinase I/glycogen synthase kinase-3beta, Proc. Natl. Acad. Sci. U. S. A. 100 (2003) 6370–6375.

[3] R. Kayed, E. Head, J. Thompson, T. McIntire, S. Milton, C. Cotman, C. Glabe, Common structure of soluble amyloid oligomers implies common mechanism of pathogenesis, Science 300 (2003) 486–489.

[4] K. Markossian, B. Kurganov, Protein folding, misfolding, and aggregation. Formation of inclusion bodies and aggresomes, Biochemistry (Moscow) 69 (2004) 971–984.

[5] N. Reixach, S. Deechongkit, X. Jiang, J. Kelly, J. Buxbaum, Tissue damage in the amyloidoses: Transthyretin monomers and nonnative oligomers are the major cytotoxic species in tissue culture, Proc. Natl. Acad. Sci. U. S. A. 101 (2004) 2817–2822.

[6] J. London, C. Skrzyna, M. Goldberg, Renaturation of *Escherichia coli* tryptophanase after exposure to 8 M urea. Evidence for the existence of nucleation centers, Eur. J. Biochem. 47 (1974) 409–415.

[7] R. Wetzel, Mutations and off-pathway aggregation of proteins, Trends Biotechnol. 12 (1994) 193–198.

[8] J. Butler, The current picture of the structure and assembly of tobacco mosaic virus, J. Gen. Virol. 65 (1984) 253–279.

[9] R. Kopito, Aggresomes, inclusion bodies and protein aggregation, Trends Cell Biol. 10 (2000) 524–530.

[10] V. Orlov, A. Arutyunyan, S. Kust, E. Litmanovich, V. Drachev, E. Dobrov, Macroscopic aggregation of tobacco mosaic virus coat protein, Biochemistry (Moscow) 66 (2001) 154–162.

[11] B. Kurganov, E. Rafikova, E. Dobrov, Kinetics of thermal aggregation of tobacco mosaic virus cost protein, Biochemistry (Moscow) 67 (2002) 525–533.

[12] E. Rafikova, B. Kurganov, A. Arutyunyan, S. Kust, V. Drachev, E. Dobrov, A mechanism of macroscopic (amorphous) aggregation of the tobacco mosaic virus coat protein, Int. J. Biochem. Cell Biol. 35 (2003) 1452–1460.

[13] E. Rafikova, Y. Panyukov, A. Arutyunyan, L. Yaguzhinsky, V. Drachev, E. Dobrov, Low sodium dodecyl sulfate concentrations inhibit tobacco mosaic virus coat protein amorphous aggregation and change the protein stability, Biochemistry (Moscow) 69 (2004) 1372–1378.

[14] Y. Panyukov, M. Nemykh, E. Rafikova, B. Kurganov, L. Yaguzhinsky, A. Arutyunyan, V. Drachev, E. Dobrov, Low cetyltrimethylammonium bromide concentrations induce reversible aggregation of tobacco mosaic virus and it's coat protein at room temperature, Int. J. Biochem. Cell Biol. 38 (2006) 533–543.

[15] R. Diaz-Avalos, D. Caspar, Hyperstable stacked-disk structure of tobacco mosaic virus protein: electron cryomicroscopy image reconstruction related to atomic models, J. Mol. Biol. 297 (2000) 67–72.

[16] F. Bassi, G. Arcovito, M. Spirito, A. Mordente, G. Martorana, Self-similarity properties of alpha-crystallin supramolecular aggregates, Biophys. J. 69 (1995) 2720–2727.

[17] U. Elofsson, P. Dejmek, M. Paulson, Heat-induced aggregation of beta-lactoglobulin studied by dynamic light scattering, Int. Dairy J. 6 (1996) 343–357.

[18] N. Santos, M. Castanho, Teaching light scattering spectroscopy: the dimension and shape of tobacco mosaic virus, Biophys. J. 71 (1996) 1641–1650.

[19] C. Bon, T. Nicolai, D. Durand, Growth and structure of aggregates of heat-denatured beta-lactoglobulin, Int. J. Food Sci. Technol. 34 (1999) 451–465.

[20] J. Schüler, J. Frank, W. Saenger, Y. Georgalis, Thermally induced aggregation of human transferrin receptor studied by light-scattering techniques, Biophys. J. 77 (1999) 1117–1125.

[21] S. Abgar, S. Vanhoudt, T. Aerts, J. Clauweart, Study of the chaperoning mechanism of bovine lens alpha-crystallin, a member of the alpha-small shock superfamily, Biophys. J. 80 (2001) 1986–1995.

[22] V. Meunier, T. Nicolai, D. Durand, Structure of aggregating kappa-carrageenan factor studied by light scattering, Int. J. Biol. Macromol. 28 (2001) 157–165.

[23] F. Bettelheim, Kinetics of chaperoning of dithiothreitol-denatured alpha-lactalbumin by alpha-crystallin, Int. J. Biol. Macromol. 30 (2002) 161–169.

[24] A. Modler, K. Gast, G. Lutsch, G. Damaschun, Assembly of amyloid protofibrils via critical oligomers — a novel pathway of amyloid formation, J. Mol. Biol. 325 (2003) 135–148.

[25] C. Follmer, F. Pereira, N. Da Silveira, C. Carlini, Jack bean urease (EC 3.5.1.5) aggregation monitored by dynamic and static light scattering, Biophys. Chem. 111 (2004) 79–87.

[26] V. Militello, C. Casarino, A. Emanuele, A. Giostra, F. Pullara, M. Leone, Aggregation kinetics of bovine serum albumin studied by FTIR spectroscopy and light scattering, Biophys. Chemist. 107 (2004) 175–187.

[27] H. Khanova, K. Markossian, B. Kurganov, A. Samoilov, S. Kleimenov, D. Levitsky, I. Yudin, A. Timofeeva, K. Muranov, M. Ostrovsky, Mechanism of chaperone-like activity. Suppression of thermal aggregation of beta-crystallin by alpha-crystallin, Biochemistry 44 (2005) 15480–15487.

[28] K. Markossian, B. Kurganov, D. Levitsky, H. Khanova, N. Chebotareva, A. Samoilov, T. Eronina, N. Fedurkina, L. Mitskevich, A. Merem'yanin, S. Kleymenov, V. Makeeva, V. Muronets, I. Naletova, I. Shalova, R. Asryants, E. Schmalhausen, L. Saso, Yu. Panyukov, E. Dobrov, I. Yudin, A. Timofeeva, K. Muranov, M. Ostrovsky, Mechanisms of chaperone-like activity, in: T.R. Obalinsky (Ed.), Protein Folding: New Research, Nova Science Publishers, Inc., New York, 2006, pp. 89–171.

[29] K.A. Markossian, H.A. Khanova, S.Y. Kleimenov, D.I. Levitsky, N.A. Chebotareva, R.A. Asryants, V.I. Muronetz, L. Saso, I.K. Yudin, B.I. Kurganov, Mechanism of thermal aggregation of rabbit muscle glyceraldehyde-3-phosphate dehydrogenase, Biochemistry 45 (2006) 13375–13384.

[30] E. Dobrov, M. Abu-Eid, A. Solovyev, S. Kust, V. Novikov, Properties of the coat protein of a new tobacco mosaic virus coat protein ts-mutant, J. Protein Chem. 16 (1997) 27–36.
[31] H. Fraenkel-Conrat, Degradation of tobacco mosaic virus with acetic acid, Virology 1 (1957) 1–4.
[32] E. Dobrov, S. Kust, O. Yakovleva, T. Tikhonenko, Structure of single-stranded virus RNA in situ. II. Optical activity of five tobacco mosaic-like viruses and their components, Biochem. Biophys. Acta 475 (1977) 623–637.
[33] S. Chiou, P. Azari, M. Himmel, P. Squire, Isolation and physical characterization of bovine lens crystallins, Int. J. Pept. Protein Res. 13 (1979) 409–417.
[34] H. Cummins, E. Pike, Photon Correlation and Light Beating Spectroscopy, Plenum Press, New York, 1974.
[35] D. Weitz, J. Huang, M. Lin, J. Sung, Limits of the fractal dimension for irreversible kinetic aggregation of gold colloids, Phys. Rev. Lett. 54 (1985) 1416–1419.
[36] D. Weitz, M. Lin, Dynamic scaling of cluster-mass distributions in kinetic colloid aggregation, Phys. Rev. Lett. 57 (1986) 2037–2040.
[37] M. Lin, H. Linsday, D. Weitz, R. Ball, R. Klein, P. Meakin, Universality of fractal aggregates as probed by light scattering, Proc. R. Soc. Lond., A Contain. Pap. Math. Phys. Character 423 (1989) 71–87.
[38] M. Berka, J.A. Rice, Relation between aggregation kinetics and the structure of kaolinite aggregates, Langmuir 21 (2005) 1223–1229.
[39] J. Horowitz, Alpha-crystallin can function as a molecular chaperone, Proc. Natl. Acad. Sci. U. S. A. 89 (1992) 10449–10453.
[40] B. Derham, J. Harding, Alpha-crystallin as a molecular chaperone, Prog. Retin. Eye Res. 18 (1999) 463–509.
[41] E. Ganea, Chaperone-like activity of alpha-crystallin and other small heat shock proteins, Curr. Protein Pept. Sci. 2 (2001) 205–225.
[42] R. Augusteyn, Alpha-crystallin: a review of its structure and function, Clin. Exp. Optom. 87 (2004) 356–366.
[43] F. Bettelheim, R. Ansari, Q. Cheng, J. Zigler, The mode of chaperoning of dithiothreitol-denatured alpha-lactalbumin by alpha-crystallin, Biochem. Biophys. Res. Commun. 261 (1999) 292–297.